Physics of runaway electrons with Shattered Pellet Injection at JET

C. Reux[1], C. Paz-Soldan[2,3], N. Eidietis[2], M. Lehnen[4], P. Aleynikov[5], S. Silburn[6], V. Bandaru[7], O. Ficker[8], M. Hoelzl[7], E.M. Hollmann[9], S. Jachmich[4], E. Joffrin[1], P.J. Lomas[6], F. Rimini[6], L. Baylor[10], A. Bleasdale[6], L. Calacci[11], F. Causa[12], D. Carnevale[11], I. Coffey[13], D. Craven[6], A. Dal Molin[14], E. de la Luna[15], G. De Tommasi[16], J. Garcia[1], T. Gebhart[10], L. Giacomelli[12], A. Huber[17], E. Khilkevich[18], C. Lowry[20], E. Macusova[8], A. Manzanares[19], M. Nocente[14], E. Panontin[14], G. Papp[7], G. Pautasso[7], A. Peacock[20], V. Plyusnin[21], A. Shevelev[18], D. Shiraki[2], C. Sommariva[22], C. Sozzi[12], S. Sridhar[1], R. Sweeney[23], G. Szepesi[6], R. A. Tinguely[23], J. Wilson[6] and JET contributors‡

[1] CEA, IRFM, F-13108 Saint-Paul-les-Durance, France

[2] General Atomics, PO Box 85608, San Diego, CA 92186-5608, United States of America

[3] Department of Applied Physics and Applied Mathematics, Columbia University, New York, New York 10027, USA

[4] ITER Organization, Route de Vinon-sur-Verdon, CS 90 046 - 13067 St Paul Lez Durance Cedex - France

[5] Max-Planck-Institut für Plasmaphysik, Greifswald, Germany

[6] CCFE, Culham Science Centre, Abingdon, Oxon, OX14 3DB, United Kingdom of Great Britain and Northern Ireland

[7] Max-Planck-Institut für Plasmaphysik, D-85748 Garching, Germany

[8] Institute of Plasma Physics of the CAS, Za Slovankou 1782/3, 182 00 Praha 8, Czech Republic

[9] University of California-San Diego, 9500 Gilman Dr., La Jolla, CA 92093-0417, United States of America

[10] Oak Ridge National Laboratory, Oak Ridge, TN 37831-6169, TN, United States of America

[11] Università di Roma Tor Vergata, Via del Politecnico 1, Roma, Italy

[12] Istituto per la Scienza e Tecnologia dei Plasmi, ISTP-CNR, via R. Cozzi 53, 20125 Milano, Italy

[13] School of Mathematics and Physics, Queen's University, Belfast, BT7 1NN, United Kingdom of Great Britain and Northern Ireland

[14] University Milano-Bicocca, Piazza della Scienza 3, 20126 Milano, Italy

[15] Laboratorio Nacional de Fusión, CIEMAT, Madrid, Spain

‡ See the author list of 'Overview of JET results for optimising ITER operation' by J. Mailloux et al. to be published in Nuclear Fusion Special issue: Overview and Summary Papers from the 28th Fusion Energy Conference (Nice, France, 10-15 May 2021)

[16] Consorzio CREATE, Via Claudio 21, 80125 Napoli, Italy
[17] Forschungszentrum Jülich GmbH, Institut für Energie und Klimaforschung, Plasmaphysik, 52425 Jülich, Germany
[18] Ioffe Physico-Technical Institute, 26 Politekhnicheskaya, St Petersburg 194021, Russian Federation
[19] Universidad Complutense de Madrid, Madrid, Spain
[20] European Commission, B-1049 Brussels, Belgium
[21] Instituto de Plasmas e Fusão Nuclear, Instituto Superior Técnico, Universidade de Lisboa, Portugal
[22] Ecole Polytechnique Fédérale de Lausanne (EPFL), Swiss Plasma Center (SPC), CH-1015 Lausanne, Switzerland
[23] Plasma Science and Fusion Center, Massachusetts Institute of Technology, Cambridge, MA 02139, United States of America

E-mail: `cedric.reux@cea.fr`

August 2021

Abstract.

Runaway electrons created during tokamak disruptions pose a threat to a reliable operation of future larger machines. Experiments using Shattered Pellet Injection (SPI) have been carried out at the JET tokamak to investigate ways to prevent their generation or suppress them if avoidance is not sufficient. Avoidance is possible if the SPI contains a sufficiently low fraction of high-Z material, or if it is fired early in advance of a disruption prone to runaway generation. These results are consistent with previous similar findings obtained with Massive Gas Injection. Suppression of an already accelerated beam is not efficient using High-Z material, but deuterium leads to harmless terminations without heat loads. This effect is the combination of a large MHD instability scattering runaway electrons on a large area and the absence of runaway regeneration during the subsequent current collapse thanks to the flushing of high-Z impurities from the runaway companion plasma. This effect also works in situations where the runaway beam moves upwards and undergoes scraping-off on the wall.

1. Introduction

Runaway electrons (REs) are the most challenging consequences of a tokamak disruption. They form multi-MA beams that may cause serious damage to the plasma-facing components. REs are accelerated by the large parallel electric fields generated by the current quench of a disruption, through the so-called primary generation mechanisms: mainly Dreicer [1] and hot-tail [2] processes. They are then multiplied by the avalanche mechanism [3, 4]. Shattered Pellet Injection (SPI) [5] is currently the baseline disruption and RE mitigation method for ITER [6]. Research on SPI follows earlier results obtained with Massive Gas Injection (MGI) as a promising way to handle disruption consequences [7, 8] and suppress both primary and secondary mechanisms. RE mitigation can be thought with two layers of defense: preventing RE generation using pre-emptive SPI or suppressing the RE beam by SPI when it is fully formed. The

present article is organized as follows: the first section is focused on the first layer of defense, with the determination of the runaway existence domain as a function of the SPI content and preemptive deuterium injection to avoid the generation of a runaway beam. The second section is devoted to the second line of defense, with the mitigation of a full-blown RE beam by high-Z SPI or Deuterium SPI. The third section focuses on the physics processes at play with the deuterium injection and the limits of its efficiency. The fourth section concludes.

2. Preventing runaway generation

2.1. Single injection: Runaway electron existence domain

The ITER disruption mitigation strategy involves SPI in most of the cases where a disruption is likely to happen [6]. Mitigating heat loads and forces requires the SPI material mix to contain a minimum fraction of high-Z material such as argon or neon. However, this high-Z material increases the odds of generating REs during the disruption. It is therefore necessary to determine a maximum amount of high-Z material which can be tolerated before an excessive amount of REs is generated. The impact of argon in the mitigation material mix was demonstrated with MGI, with increasing fractions of argon generating increasing RE currents [8]. A similar experiment was replicated with SPI on JET, showing the same qualitative behaviour as shown on figure 1 for diverted plasmas. Increasing argon content and toroidal magnetic field both lead to higher amounts of runaways, with the boundary of the existence domain below 1.8 T for pure argon and 3.0 T for 10 to 20% argon. The location of those boundaries is compatible with earlier results with MGI. Runaway currents inside the existence domain are lower with MGI, but could be due to the difference in gas dynamics and total amounts of material injected. Earlier MGI experiments injected ≈800 Pa.m^3 (2.0×10^{23} atoms) but with a gas front spread in space, to be compared with 50 to 70 Pa.m^3 (1.3×10^{22} to 1.8×10^{22} atoms) injected by SPI but with a supposedly steeper mixing front. Results in limited configurations are similar.

2.2. Double injection: preventing runaway generation

If runaway generation of an incoming disruption is very likely, injecting a large amount of deuterium just before the thermal quench (TQ) can also be foreseen as a prevention method and was demonstrated for JET [8]. Injecting large amounts of deuterium shortly before the disruption can also be thought as a way of pre-cooling the plasma by dilution to decrease heat fluxes during the thermal quench as well as reducing the hot tail primary RE generation effect [9]. This method was tried using a deuterium shattered pellet fired at various times around the thermal quench of a disruption likely to produce REs. This disruption is triggered by a small quantity of argon (3-7 Pa.m^3). Figure 2 shows that as long as the pellet arrives at the plasma edge before the thermal quench, RE generation is prevented or limited to small amounts only visible as a small burst of

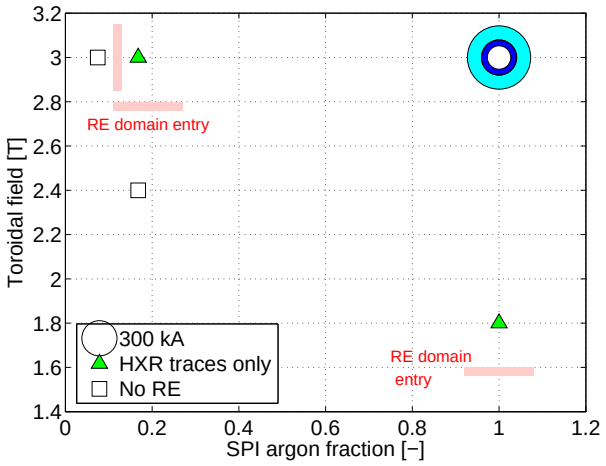

Figure 1. Runaway electron existence domain on JET as a function of the toroidal field and argon fraction for diverted configurations. Square symbols are cases without REs. Triangle symbols are cases where no measurable RE current is observed but RE presence is confirmed by HXR spikes. Circle symbols are cases where a measurable RE current is observed. The size of the circle is proportional to RE current, with blue-colored rings indicating error bars.

photoneutrons. Conversely, a full-blown runaway beam is generated (with measurable runaway currents) if the pellet plume reaches the plasma edge after the thermal quench, indicating either that SPI material mixing is poor after the thermal quench or that primary mechanisms are suppressed by an early deuterium injection. This is particularly true for very early deuterium injections which compete with the argon used to trigger the original disruption, thus altering the disruption dynamics. If the pellet is larger (300 Pa.m^3 vs. 85 Pa.m^3), RE generation can still prevented even if the pellet arrives at the plasma edge 3 ms after the thermal quench as shown on figure 2. Some post-TQ prevention efficiency can however be retained if the pellet is larger (300 Pa.m^3 vs. 85 Pa.m^3) as shown on figure 2. This possibly hints at the mixing efficiency being the key effect in this prevention method. It is to be noted though that photoneutrons were completely absent with similar experiments using MGI instead of SPI. This could be due to the different mixing dynamics of SPI or to the fact that a slower valve was used to inject the argon to trigger the disruption in the MGI cases.

3. Mitigation of runaway electron beams with SPI

If runaway generation cannot be prevented by either of the methods described in the previous section, the mitigation of a full-blown runaway beam becomes necessary as a second layer of defense. A runaway beam scenario was therefore developed at JET to test various mitigations methods. The position stability of the beam was improved compared to earlier scenario which were vertically unstable [8]. In particular the observer of the vertical position control system was improved [10] and additional flux was provided to the beam by the external poloidal field control coils to sustain the current. The central

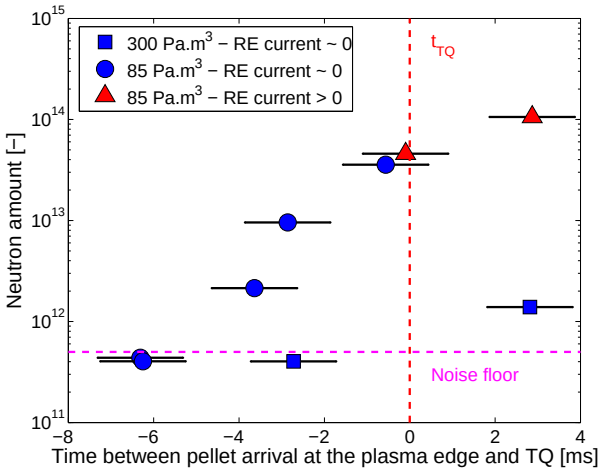

Figure 2. Photoneutron amounts versus time span between SPI arrival at the plasma edge and TQ. Measurable RE currents indicated by red triangles only occur when the pellet arrives close or after TQ.

solenoid was indeed already at maximum voltage. The resulting runaway beam lasts about one second at 500 kA current.

3.1. High-Z shattered pellet injection

High-Z material (neon, argon) was initially considered thanks to successful results on small tokamaks [11]. The result is shown on figure 3. Both neon and argon shorten the duration of the runaway beam (500 ms instead of 1 s) by accelerating the current decay. The decay rate is slightly higher with larger pellets (5 MA/s versus 9 MA/s for 68 Pa.m^3 versus 244 Pa.m^3 argon respectively), and larger with argon than neon. Photoneutron production increases when the pellet reaches the plasma, indicating runaway losses by collisions and pitch angle scattering. Radiated power increases from 1 MW to 6-10 MW, indicating that the thermal radiation from argon and neon is most probably a loss channel for the dissipated RE energy. The beam is vertically destabilized and terminates on the JET upper plasma facing components. Heat loads are recorded by infrared cameras in all cases, with no clear dependency on neither the injected species nor their amount.

A comparison of MGI versus SPI is shown on figure 4 where two similar amounts of material were injected on the same runaway beam. The dissipation occurs in the same way for both cases: radiated power increase, vertical destabilization, increased photoneutron production and heat loads at termination. This shows that SPI at JET has no obvious advantage over MGI for in-flight RE beam mitigation using argon or neon.

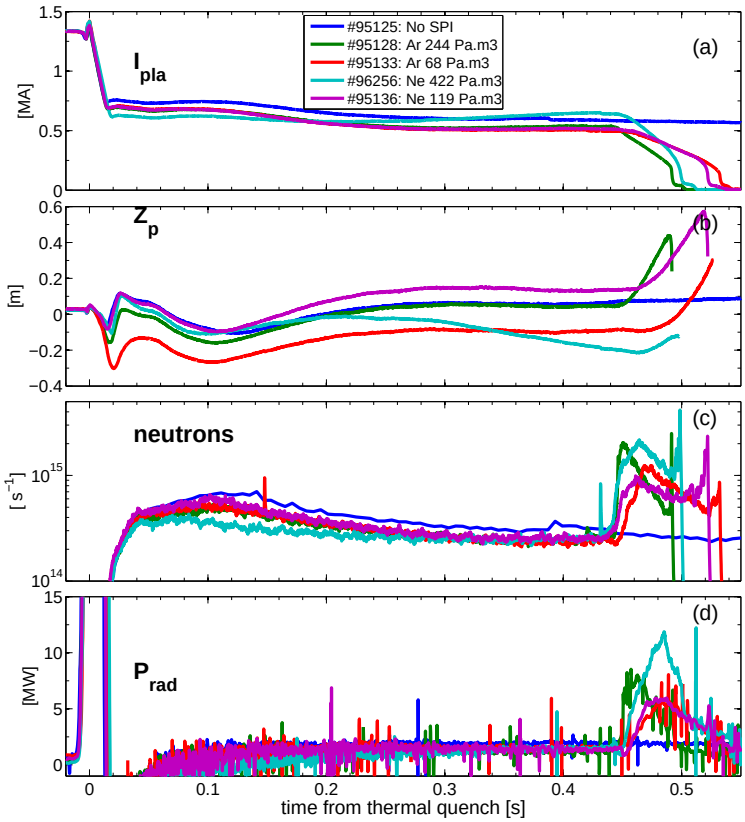

Figure 3. RE beam mitigation using argon and neon compared to a non-mitigated case. SPI is triggered 0.4 s after the thermal quench. (a) Total current. (b) Magnetic centroid vertical position. (c) photoneutrons rate (d) total radiated power

3.2. Deuterium shattered pellet injection

A D_2 injection leads to the opposite situation as shown on Fig.5: the current increases, free electron density drops to non-measurable values (below 10^{18} m^{-3} , indicating plasma recombination. This feature was previously observed on DIII-D [12], AUG [13] and COMPASS [14]. Line radiation changes from being dominated by argon lines to being dominated by deuterium lines. This shows that the argon has been flushed out of the plasma, similarly to what was observed and modelled on DIII-D [11, 15]. Photoneutron production also drops to very low values. A number of physical effects can explain this observation: the flushing-out of high-Z material reduces RE bremsstrahlung which in turn reduces photoneutron production. The reduction of pitch-angle scattering reduces runaway losses, which can also reduce photoneutron production. A decrease of RE energy cannot be excluded either. This is however less likely because the energy threshold for photoneutron production is lower for deuterium (2.2 MeV [16]) than argon (9.9 MeV [17]), so a deuterium-dominated plasma could theoretically produce more photoneutrons for a given RE energy distribution. After the pellet arrival, the synchrotron pattern changes with island chains reorganization [18]. Radiated power increases significantly from 1 MW to 4 MW and then slowly decays. This point is of

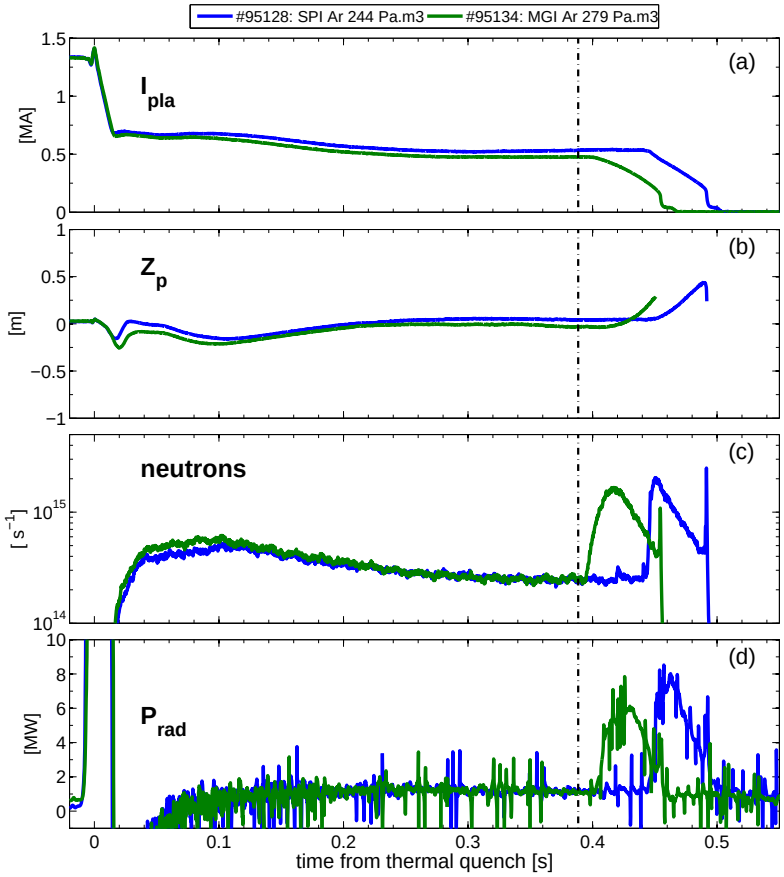

Figure 4. Comparison of RE beam mitigation with SPI and MGI. The vertical dashed line indicates the SPI and MGI firing time. MGI flight time is shorter than SPI flight time due its position with respect to the vacuum vessel, explaining the slightly earlier effect on the plasma. (a) Total current. (b) Magnetic centroid vertical position. (c) photoneutrons rate (d) total radiated power

particular interest since no increase of radiated power following the deuterium injection was observed on other machines (DIII-D, AUG, Compass, TCV). The flushing out of argon was modelled using a 1D diffusion code [19]. The code takes into account all ionization stages of argon and deuterium species. It determines the electron temperature and RE electron density (assuming the RE collisional losses are equal to the total thermal radiation) from the measured radiated power. It then computes the densities of every ion and neutral species using diffusion equations, including atomic physics as detailed in reference [19]. The radiated power profile is here taken as Gaussian with 0.3m width, which is qualitatively consistent with tomographic reconstructions of bolometry measurements. The code is able to reproduce a partial flushing out of argon and the drop of the companion plasma temperature (see figure 6), but not down to recombination. Kinetic parameters close to the measured values ($n_e \approx 10^{18} m^{-3}$, $T_e \approx 1eV$ and recombined plasma) can only be approached by artificially decreasing the measured radiated power (used as an input to compute the electron temperature) by 2 orders of magnitude as shown on figure 7. This means that the high radiated

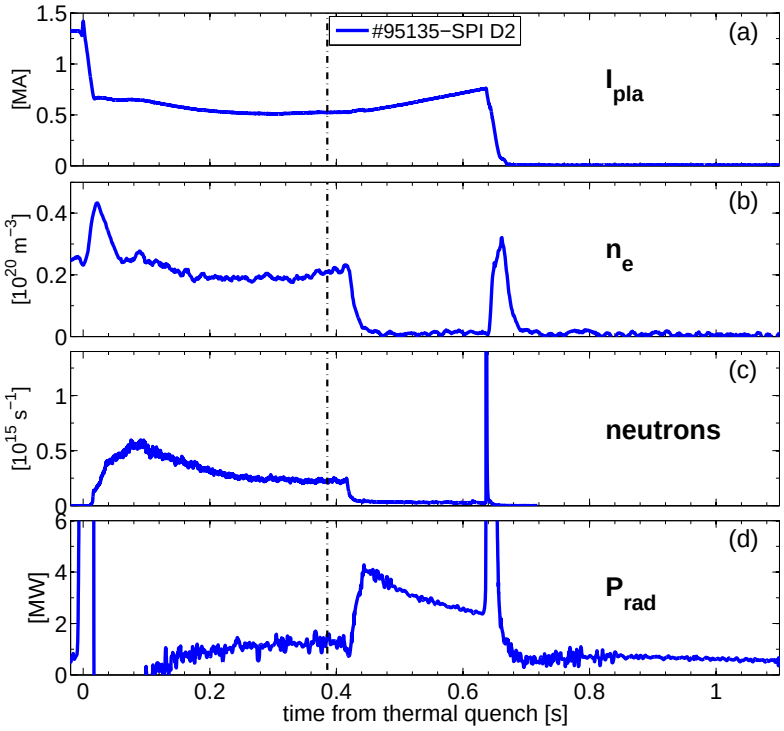

Figure 5. Overview of a D_2e-mitigated RE beam (#95135). The SPI trigger is indicated by the dashed vertical line. (a) Total current (b) Free electron density. (c) Neutron flux. (d) Total radiated power

power measured on JET comes from non-thermal sources, namely the direct interaction between runaway electrons and the companion plasma and neutrals. This behaviour was also proposed on ITER cases in reference [20].

The RE beam disappears 250 ms after the pellet arrival in a violent MHD instability. Synchrotron emission from the RE beam vanishes in less than a millisecond and a large but brief photoneuton spike is recorded. The rest of the current decay is similar to the current quench of a standard disruption with a radiated power spike. VUV spectra are no longer dominated by deuterium lines, but by argon lines as before the SPI arrival. In some cases, a current spike similar to the one observed during the thermal quench of hot plasma disruptions is visible, possibly indicating strong reorganization of the current profile and stochastization of the flux surfaces. The most prominent feature of those disruptions is the absence of measurable heat loads when runaways disappear as recorded by IR thermography, shown on Fig.8. Runaways currents up to 1.4 MA are dissipated benignly with deuterium. This is to be compared the 10 MJ.m$^-$2 deposited on the first wall for RE currents as low as 400 kA without mitigation. Figure 8 also shows that high-Z mitigation (argon or neon) is not more efficient than an absence of mitigation, and that the main dependency of heat loads of unmitigated cases is the runaway current remaining when the final wall impact occurs.

This benign termination called thereafter the "D_2 effect" is due to two processes: a large MHD instability and the absence of RE regeneration during the subsequent current

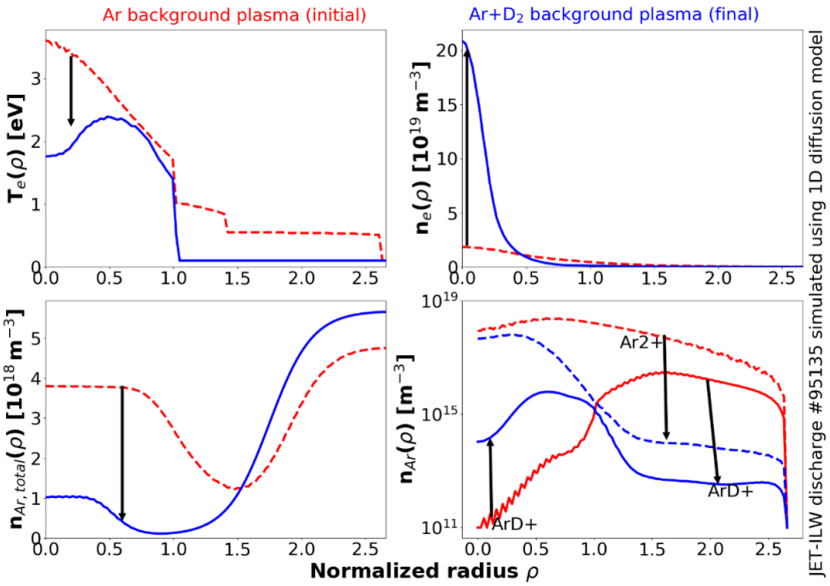

Figure 6. Kinetic profiles from a 1D-diffusion simulation of JET pulse #95135, with red traces are before the deuterium pellet arrival and blue traces are after the arrival. The simulation domain extends to the open field line region $\rho > 1$. (a) Electron temperature (b) free electron density (c) total argon density (d) density of Ar^{2+} and ArD^{+} (ionized ArD molecule)

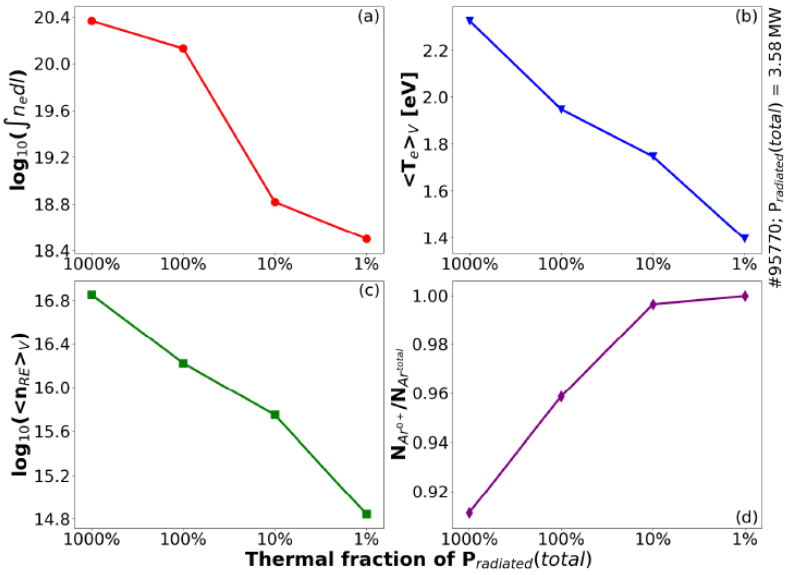

Figure 7. Profile-averaged quantities of the simulation of JET pulse #95770 as a function of the fraction of total radiated power considered as thermal (100% meaning that all radiated power is thermal and higher values are for exploration only) (a) Free electron density (experimental values are lower than 10^{18} m^{-2}) (b) averaged temperature (c) RE density (d) ratio of neutral argon over total argon.

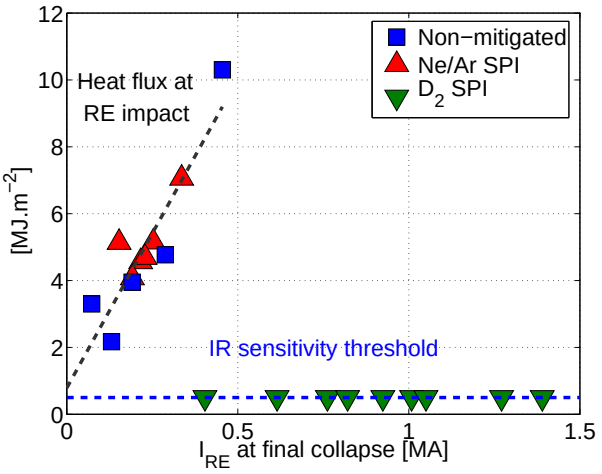

Figure 8. Heat loads from IR thermography versus RE current at collapse

quench which will be developed in the next sections.

4. The deuterium effect

4.1. MHD instability

The MHD instability dissipating REs develops without clear precursors and reaches its peak magnitude in less than 100 μs. No rotating mode is observed before the MHD burst, although seemingly locked magnetic islands are visible on the synchrotron images during the current rise between the SPI arrival and the final collapse. m=6, m=5 and m=4 (briefly) patterns are observed moving outwards, consistently with the current rise as detailed in reference [21]. The main instability itself is too short to produce a clear coherent mode visible on the Mirnov coils, but an MHD spectrum analysis of the remnants of the main instability a few tens of ms after the main spike show that n=1 is the most likely mode as shown on figure 9

The SOFT code [22] was used to give constraints on the runaway current profile by comparing synthetic synchrotron images with IR and visible camera measurements. Different current profiles, pitch angles and monoenergetic RE distributions were tested to get the best match. The match has only a weak dependency on RE energy and pitch angle. Angles from 0.1 to 0.3 and energies less than 15 MeV are the most likely parameters. The current profile is the main dependency. The best match was obtained for hollow current profiles: no combination of a peaked profile and any value of energy and pitch angle was found that could match the observations. It is however true than only mono-pitch and mono-energy RE beams were tested. However, the weak dependency of the image pattern on the RE energy and pitch angle gives confidence that current profile is the critical parameter to match the measurement. The hollowness of the current profile is also partly confirmed by the position of the islands on the IR pictures. Two distinct m=5 patterns can be briefly seen during the current rise as

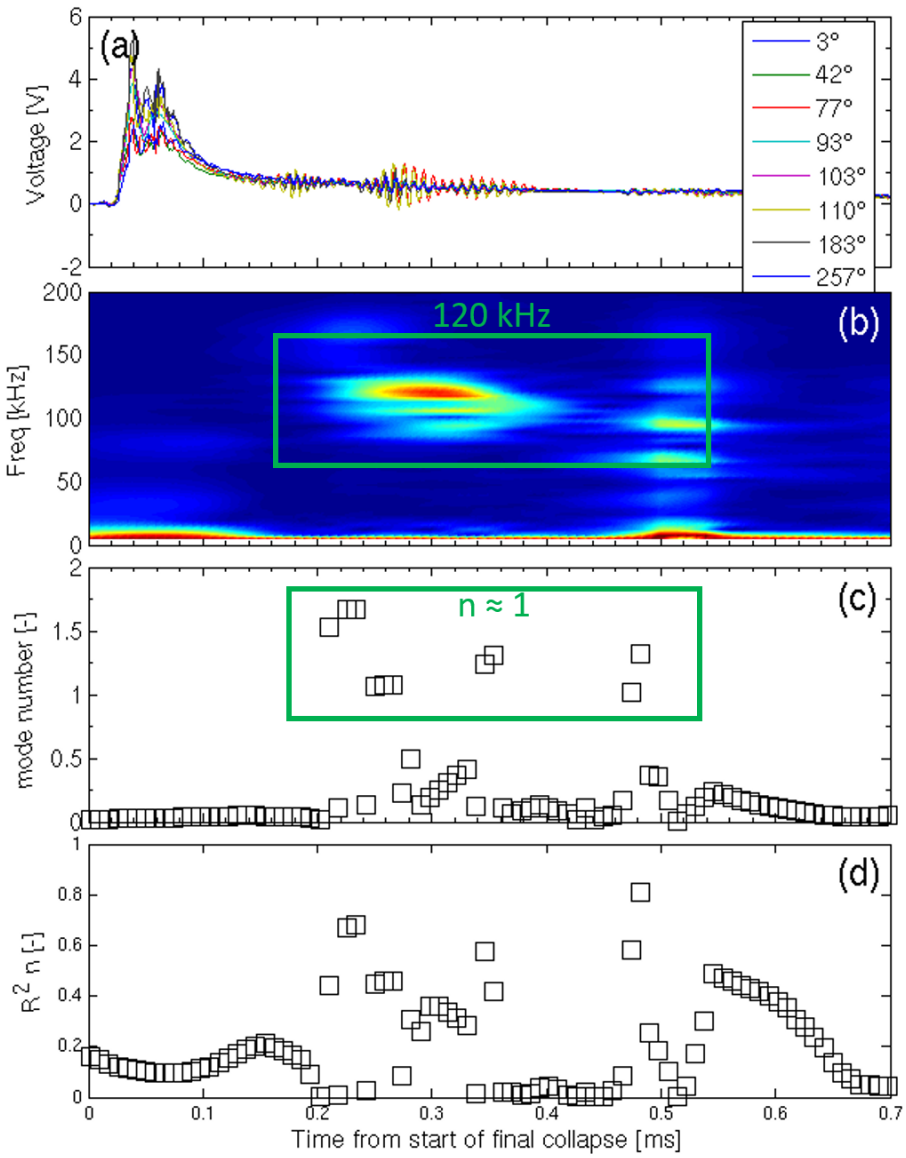

Figure 9. MHD Mirnov analysis of the remnants of the large MHD instability which dissipated the runaways. The remnant mode frequency is 120 kHz. (a) MHD coil voltage signal with their toroidal angular position (b) Spectrogram of the 257° coil (c) n mode number (d) n mode number fit quality (coefficient of determination)

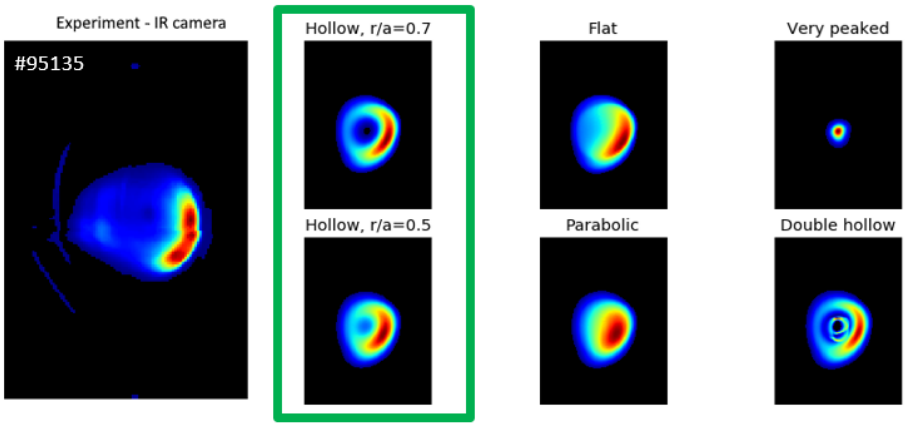

Figure 10. Measured infrared synchrotron emission (left picture) versus reconstructions made by SOFT using various current profiles. Hollow profiles (green-squared pictures) provide the best match

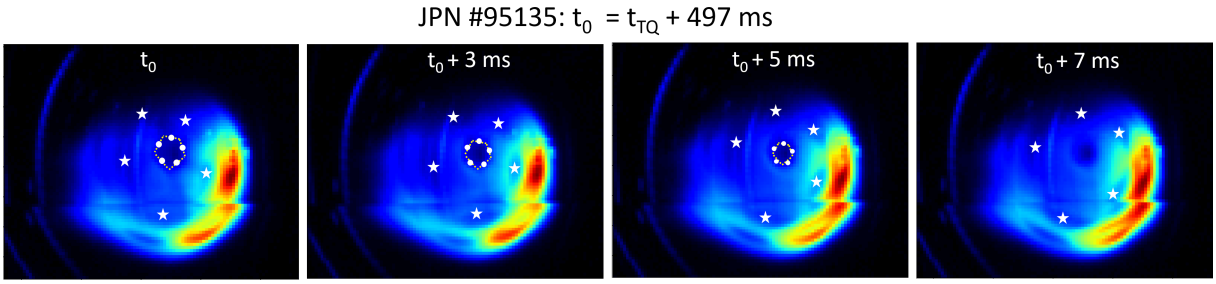

Figure 11. Synchrotron emission as seen by a tangential infrared camera showing the two m=5 island-like patterns in the emission at different times during the current rise preceding the RE beam final collapse. White stars roughly indicate the island centers of the outermost m=5 pattern, while white circles show the probable location of the island centers of the innermost m=5 pattern. The latter is mostly visible by the 5-sided dark spot in the center of the synchrotron pattern, which is highlighted by yellow dashed eye-guiding lines. Note that the m=6 outermost pattern is also visible near the edge.

shown on figure 11. The innermost m=5 pattern is only visible by the 5-sided dark spot at the center of the synchrotron pattern while the outermost pattern shows clear island-like structures. The innermost pattern moves inwards while the outermost moves outwards as is expected if the shape of the hollow current profile remains frozen while the total current increases. Other examples of inward-moving islands can be found in the pulse series described in reference [18]. Work is also in progress to understand the physics mechanisms leading to a RE hollow profile.

The termination itself usually happens at low edge safety factors as shown on figure 12, but this is not specific to benign terminations induced by the D2 effect. It does not happen only at q_{edge}=2 as observed on DIII-D [12]. This suggests that the collapse is not necessarily a low-q current instability (kink mode), and further reinforces the assumption of a hollow current profile which can produce tearing modes that could

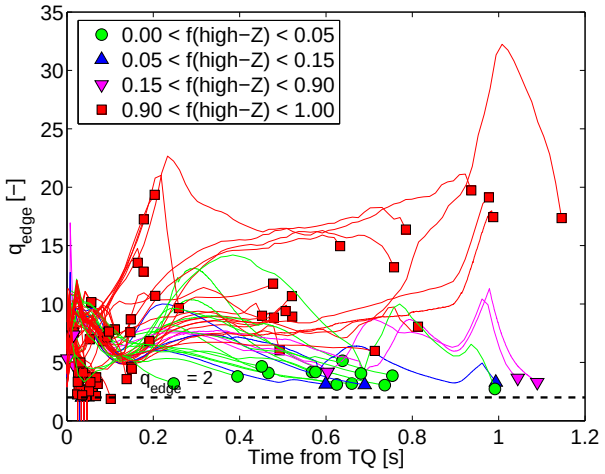

Figure 12. Edge safety factor from EFIT as a function of time during the runaway beam for various high-Z impurity ratios in the companion plasma. The impurity ratio is defined by the amount of hydrogenic species over the total amount of injected material: hydrogenic species and any neon, argon, krypton or xenon injected by either MGI or SPI both with the single RE-beam triggering injection or with a mitigation injection. Markers indicate q_{edge} at the time of beam termination.

cause the runaway beam collapse at higher edge safety factor.

The amplitude of the instability was analszed using Mirnov coils on the low-field side of the torus. They show that the amplitude of the instability $\frac{\delta B_{pol}}{B_{pol}}$ normalized to the distance to the coil is very weakly correlated to the use of deuterium (benign terminations) or not (non-benign terminations) as shown on figure 13. However, the normalized growth rate of the instability $\frac{dB_{pol}}{dt}$ is better correlated to benign terminations as shown on figure 14, although not perfectly. This shows that MHD is not the only physics process required to obtain a harmless RE dissipation.

The profile determined by the SOFT analysis was used for JOREK [23, 24] 3D MHD simulations using a RE fluid model [21]. The simulation shows a complete stochastization of the magnetic surfaces by a double tearing mode, leading to the loss of confinement and the loss of 95% of the REs in ≈ 100 μs as shown in details in reference [21]. This timescale is quantitatively compatible with the experimental observations [21]. The RE loss footprint is also enlarged by stochastization.

4.2. RE regeneration

The second prominent feature of the benign termination scenario is the fact that REs are not re-generated during the subsequent RE collapse. The high-Z material (argon in the present case) initially contained in the companion plasma is indeed almost completely flushed out by the D_2 injection. However, traces of argon remain in the background neutrals, because argon VUV lines reappear when runaways are lost during the large MHD event. The maximum radiated power normalized to the initial magnetic energy contained in the runaway beam before its dissipation is correlated to the concentration of

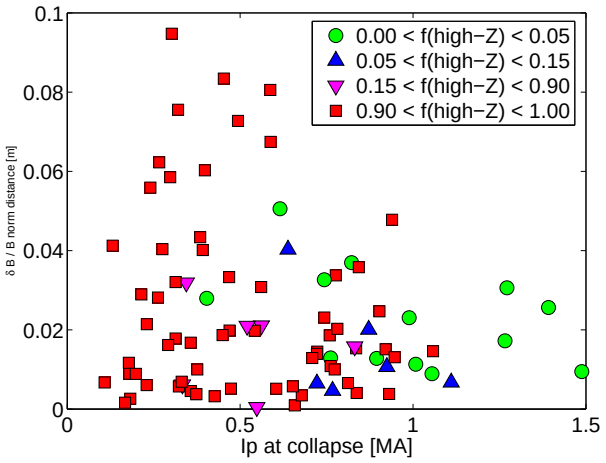

Figure 13. Amplitude of the final instability normalized to poloidal field and distance d from the beam centroid to the sensor $d_{sensor}\frac{\delta B_{pol}}{B}$ as a function of beam current at collapse

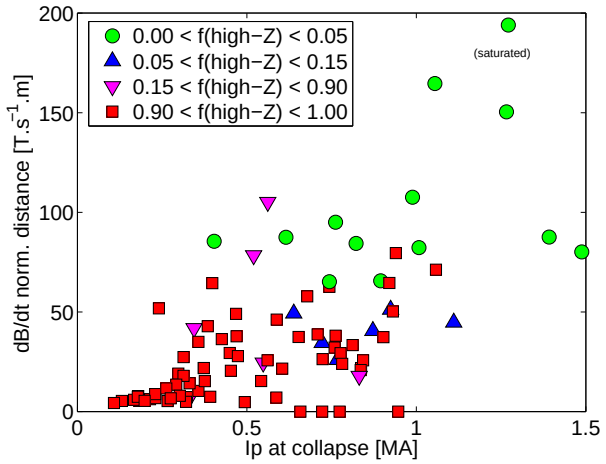

Figure 14. Growth rate of the final instability normalized to the distance d from the beam centroid to the sensor $d_{sensor}\frac{dB}{dt}$ as a function of beam current at collapse

argon in the injected material (argon injected to trigger the disruption and deuterium from SPI) as shown on figure 15. A small runaway beam detected by synchrotron emissions is also regenerated during the final collapse if the argon concentration is large enough. Increasing the argon amount further leads to an incomplete dissipation of the RE beam, and the regeneration of a full secondary beam at lower current. Several consecutive collapses may then occur until the beam is fully dissipated, sometimes with heat loads.

A 0D modelling computing self-consistently the plasma current, RE current, vessel current, electric field and plasma temperature [25, 26] was compared to the experimental observations. It shows that an argon purge ratio of 10 to 300 is needed to account for the current quench rate, and that the RE avalanche rate increases with the argon

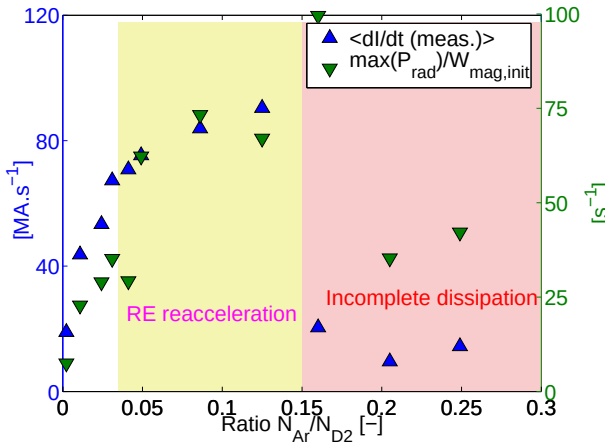

Figure 15. Current quench rate of the final collapse and maximum radiated power versus the initial Ar/D_2 ratio. 3 regimes can be identified: no regeneration, RE reacceleration, incomplete dissipation with continuous regeneration

concentration. The RE avalanche remains however low, so this model cannot conclude if the purge level would be sufficient on an ITER plasma.

Another way to interpret the observations is to compute the power balance of the runaway beam and companion plasma during the collapse. The method was proposed in ref. [27] and is further developed in the present article. The calculation assumes that the magnetic energy dissipated during runaway loss events as characterized by neutron spikes is lost through 3 different channels: inductive coupling to passive structures and coils, conversion into thermal energy in the companion plasma through Joule heating (and then radiated away), and converted into RE kinetic energy through RE regeneration. The magnetic energy contained by a MA-level runaway beam being one order of magnitude larger than its initial kinetic energy, the conversion rate is of critical importance to the damage risk posed by RE beams. This power balance is shown on figure 16, and reveals that the conversion rate is much lower for RE beams with low high-Z contents, which are also correlated with benign RE dissipation. This shows that high-Z impurities contribute to the conversion of magnetic energy into kinetic energy, and explains the higher heat loads in those cases.

4.3. The deuterium effect in a vertically moving beam

A RE beam on ITER is expected to be vertically unstable due to the slow reaction time of the control system to abrupt current changes [28]. This can lead to a situation where the RE beam scrapes off the wall thus losing its energy continuously on its contact point [29]. In order to test if this effect can reduce the efficiency of the D2 SPI, a standard runaway beam scenario was deliberately sent to the upper dump plate using a kick from the vertical control system. The D2 SPI was then fired at various times during the ensuing vertical displacement. Four typical cases are shown on figure 17. The temperature as measured by an infrared camera in the various cases tested is shown on

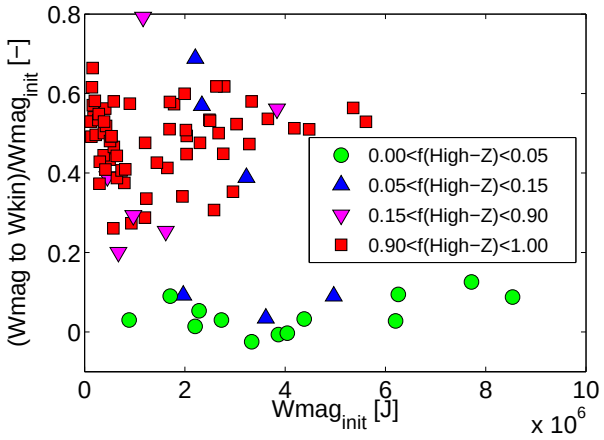

Figure 16. Fraction of magnetic energy converted into kinetic energy normalized to the initial magnetic energy carried by the RE beam as a function of the initial magnetic energy carried by the beam for various fractions of high-Z impurities in the companion plasma

figure 18. If enough time is left for the deuterium to flush-out impurities, sending the beam into a vertical displacement retains a benign termination (green case on figure 17). It is worth noting that unlike the D2-induced collapses of vertically stable beams, RE losses do not happen in a single neutron burst, which used to be characteristic of non-benign terminations. It is yet unclear if this is the sign of an efficiency roll-over or simply due to the dynamics of the termination related to the hollow current profile. The D2 effect still works if the vertical displacement starts at the same time as the arrival of the pellet in the plasma (blue case on figure 17, since the purge takes approximately the same time (20 ms) as the VDE (15 ms). If the D2 pellet arrives too late in the vertical displacement (red case on figure 17) then heat loads start to rise, indicating insufficent dissipation. The vertical speed is also faster and close to the one of an unmitigated VDE (see figure 17) and the density rise lower, possibly indicating poorer mixing. Interestingly, the heat load footprint of this intermediate case between benign and non-mitigated cases is larger than the non-mitigated cases. This may due to a large enough MHD instability to spread heat loads, but enough high-Z impurities to regenerate a significant amount of REs, leasing to larger heat loads.

5. Conclusions and discussion

Experiments at JET show that SPI can avoid REs if injected before the triggering of the disruption if the pre-emptive pellet contains enough D_2 or is injected early enough before the disruption. Suppressing a fully-formed RE beam is not effective using high-Z SPI species and leads to heat loads on the wall, not differently from a non-mitigated RE beam. SPI is equivalent to MGI in that respect. Conversely, D_2 SPI leads to benign terminations of beams up to 1.4 MA. This is due to the combination of a large MHD instability and the absence of regeneration of REs thanks to a clean companion

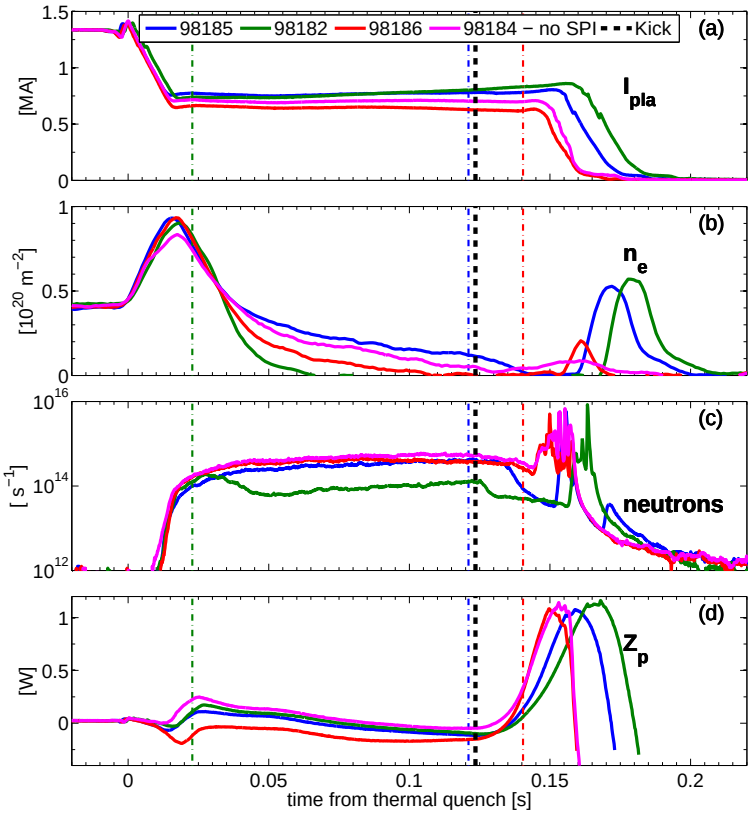

Figure 17. Mitigation of a vertically unstable RE beam with deuterium. Thin vertical dashed lines indicate the pellet arrival time. The thick vertical dashed line is the vertical kick time. (a) Total current (b) Free electron density (c) neutron rate (d) vertical position of the current centroid

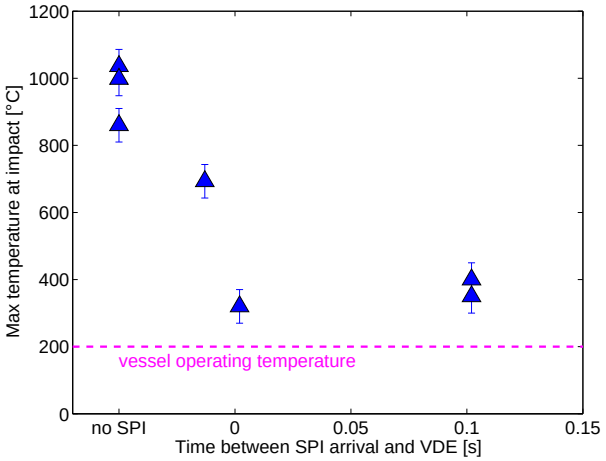

Figure 18. RE impact temperature as a function of the delay between the SPI arrival and the start of the vertical displacement event.

plasma. The MHD instability develops from a hollow current profile as deduced from the island patterns on infrared images, from the fact that $q_{edge} \geq 2$ and the comparison of measured synchrotron emissions with the SOFT code. REs are dissipated in a few tens of microseconds, which is reproduced by JOREK simulations. The role of high-Z impurities in the RE regeneration during the final collapse is confirmed by the observations of the gradual reappearance of increasingly large runaway beams when the concentration of argon is increased. If the argon content is too large, only an incomplete dissipation of the runaway beam occurs. A secondary beam is then produced, reaccelerated and undergoes multiple intermediate collapses until the final loss which may occur with measurable heat loads. The importance of the high-Z impurity concentration is further underlined by the fact it promotes conversion of the RE magnetic energy to kinetic energy, which is ultimately the main source of damage. The D2 effect is still efficient when the beam is vertically destabilized as it will be on ITER.

This RE dissipation scenario is promising for future machines as it offers a good second line of defense for runaway beams, and was found to be efficient on the tokamak which currently has the largest RE avalanche amplification factor: JET. The extrapolation to ITER is still an open question since the high-Z purge required to prevent regeneration on an ITER plasma will be higher given the foreseen avalanche gains. More simulations of the RE regeneration is such events are therefore required. The initial dissipation of the RE beam by the MHD instability will also need to leave as few RE seeds as possible since these will be strongly amplified by the avalanche in ITER. More MHD simulations are therefore underway to test the scenario on ITER.

However, even if some partial regeneration occurs as it did on JET with high concentrations of high-Z impurities, repetitive injections of D_2 pellets using the multiple SPI barrels planned on ITER could decrease the current stepwise down to an acceptable level.

Acknowledgments

This work has been carried out within the framework of the EUROfusion Consortium and has received funding from the Euratom research and training programme 2014-2018 and 2019-2020 under grant agreement No 633053. The views and opinions expressed herein do not necessarily reflect those of the European Commission. The JET SPI project is a collaborative effort of EURATOM, the ITER Organization, and the US Department of Energy. It received funding from the ITER Organization. The views and opinions expressed herein do not necessarily reflect those of the ITER Organization. This material is based upon work supported by the U.S. Department of Energy, Office of Science, Office of Fusion Energy Sciences, under Award No. DE-SC0020299.

[1] H. Dreicer. Electron and ion runaway in a fully ionized gas. i. *Phys. Rev.*, 115(2):238–249, Jul 1959.

[2] H. M. Smith and E. Verwichte. Hot tail runaway electron generation in tokamak disruptions. *Physics of Plasmas*, 15(7):072502, 2008.

[3] M.N Rosenbluth and S.V Putvinski. Theory for avalanche of runaway electrons in tokamaks. *Nuclear Fusion*, 37(10):1355–1362, oct 1997.

[4] Boris N. Breizman, Pavel Aleynikov, Eric M. Hollmann, and Michael Lehnen. Physics of runaway electrons in tokamaks. *Nuclear Fusion*, 59(8):083001, jun 2019.

[5] L.R. Baylor, S.J. Meitner, T.E. Gebhart, J.B.O. Caughman, J.L. Herfindal, D. Shiraki, and D.L. Youchison. Shattered pellet injection technology design and characterization for disruption mitigation experiments. *Nuclear Fusion*, 59(6):066008, apr 2019.

[6] M. Lehnen, D.J. Campbell, D. Hu, U. Kruezi, T.C. Luce, S. Maruyama, J.A. Snipes, and R. Sweeney. R and d for reliable disruption mitigation in iter. IAEA, Oct 2018.

[7] D. G. Whyte, T. C. Jernigan, D. A. Humphreys, A. W. Hyatt, C. J. Lasnier, P. B. Parks, T. E. Evans, M. N. Rosenbluth, P. L. Taylor, A. G. Kellman, D. S. Gray, E. M. Hollmann, and S. K. Combs. Mitigation of tokamak disruptions using high-pressure gas injection. *Phys. Rev. Lett.*, 89:055001, Jul 2002.

[8] C. Reux, V. Plyusnin, B. Alper, D. Alves, B. Bazylev, E. Belonohy, A. Boboc, S. Brezinsek, I. Coffey, J. Decker, P. Drewelow, S. Devaux, P.C. de Vries, A. Fil, S. Gerasimov, L. Giacomelli, S. Jachmich, E.M. Khilkevitch, V. Kiptily, R. Koslowski, U. Kruezi, M. Lehnen, I. Lupelli, P.J. Lomas, A. Manzanares, A. Martin De Aguilera, G.F. Matthews, J. Mlynář, E. Nardon, E. Nilsson, C. Perez von Thun, V. Riccardo, F. Saint-Laurent, A.E. Shevelev, G. Sips, and C. Sozzi and. Runaway electron beam generation and mitigation during disruptions at JET-ILW. *Nuclear Fusion*, 55(9):093013, aug 2015.

[9] E. Nardon, D. Hu, M. Hoelzl, and D. Bonfiglio and. Fast plasma dilution in ITER with pure deuterium shattered pellet injection. *Nuclear Fusion*, 60(12):126040, oct 2020.

[10] D Carnevale, M Ariola, G Artaserse, F Bagnato, W Bin, L Boncagni, T Bolzonella, F Bombarda, P Buratti, L Calacci, F Causa, S Coda, F Cordella, J Decker, G De Tommasi, B Duval, B Esposito, G Ferrò, O Ficker, L Gabellieri, A Gabrielli, S Galeani, C Galperti, S Garavaglia, A Havranek, M Gobbin, M Gospodarczyk, G Granucci, E Joffrin, M Lennholm, A Lier, E Macusova, F Martinelli, J R Martìn-Solìs, J Mlynar, L Panaccione, G Papp, M Passeri, G Pautasso, Ž Popovic, C Possieri, G Pucella, U A Sheikh, G Ramogida, C Reux, F Rimini, A Romano, M Sassano, B Tilia, O Tudisco, D Valcarcel, , and and. Runaway electron beam control. *Plasma Physics and Controlled Fusion*, 61(1):014036, nov 2018.

[11] D. Shiraki, N. Commaux, L.R. Baylor, C.M. Cooper, N.W. Eidietis, E.M. Hollmann, C. Paz-Soldan, S.K. Combs, and S.J. Meitner. Dissipation of post-disruption runaway electron plateaus by shattered pellet injection in DIII-d. *Nuclear Fusion*, 58(5):056006, mar 2018.

[12] C Paz-Soldan, N W Eidietis, Y Q Liu, D Shiraki, A H Boozer, E M Hollmann, C C Kim, and A Lvovskiy. Kink instabilities of the post-disruption runaway electron beam at low safety factor. *Plasma Physics and Controlled Fusion*, 61(5):054001, mar 2019.

[13] G. Pautasso, M. Dibon, M. Dunne, R. Dux, E. Fable, P. Lang, O. Linder, A. Mlynek, G. Papp, M. Bernert, A. Gude, M. Lehnen, P.J. McCarthy, J. Stober, and and. Generation and dissipation of runaway electrons in ASDEX upgrade experiments. *Nuclear Fusion*, 60(8):086011, jul 2020.

[14] J Mlynar, O Ficker, E Macusova, T Markovic, D Naydenkova, G Papp, J Urban, M Vlainic, P Vondracek, V Weinzettl, O Bogar, D Bren, D Carnevale, A Casolari, J Cerovsky, M Farnik, M Gobbin, M Gospodarczyk, M Hron, P Kulhanek, J Havlicek, A Havranek, M Imrisek, M Jakubowski, N Lamas, V Linhart, K Malinowski, M Marcisovsky, E Matveeva, R Panek, V V Plyusnin, M Rabinski, V Svoboda, P Svihra, J Varju, and J Zebrowski and. Runaway electron experiments at COMPASS in support of the EUROfusion ITER physics research. *Plasma Physics and Controlled Fusion*, 61(1):014010, nov 2018.

[15] E. M. Hollmann, I. Bykov, N. W. Eidietis, J. L. Herfindal, A. Lvovskiy, R. A. Moyer, P. B. Parks, C. Paz-Soldan, A. Yu. Pigarov, D. L. Rudakov, D. Shiraki, and J. Watkins. Study of argon expulsion from the post-disruption runaway electron plateau following low-z massive gas injection in diii-d. *Physics of Plasmas*, 27(4):042515, 2020.

[16] R. Sher, J. Halpern, and A. K. Mann. Photoneutron thresholds. *Phys. Rev.*, 84:387–394, Nov

1951.

[17] B. E. Carlson, N. G. Lehtinen, and U. S. Inan. Neutron production in terrestrial gamma ray flashes. *Journal of Geophysical Research: Space Physics*, 115(A4), 2010.

[18] C. Sommariva. *To be submitted.*

[19] E.M. Hollmann, N.W. Eidietis, J.L. Herfindal, P.B. Parks, A.Y. Pigarov, D. Shiraki, M.E. Austin, L. Bardoczi, L. Baylor, I. Bykov, T.N. Carlstrom, D. Kaplan, C.J. Lasnier, A. Lvovskiy, A. Moser, R.A. Moyer, C. Paz-Soldan, D.L. Rudakov, C. Samuell, M. Shafer, M. Van Zeeland, A. Welander, and R. Wilcox. Study of argon assimilation into the post-disruption runaway electron plateau in DIII-d and comparison with a 1d diffusion model. *Nuclear Fusion*, 59(10):106014, aug 2019.

[20] Nathan A. Garland, Hyun-Kyung Chung, Christopher J. Fontes, Mark C. Zammit, James Colgan, Todd Elder, Christopher J. McDevitt, Timothy M. Wildey, and Xian-Zhu Tang. Impact of a minority relativistic electron tail interacting with a thermal plasma containing high-atomic-number impurities. *Physics of Plasmas*, 27(4):040702, 2020.

[21] V Bandaru, M Hoelzl, C Reux, O Ficker, S Silburn, M Lehnen, N Eidietis, and JOREK Team. Magnetohydrodynamic simulations of runaway electron beam termination in JET. *Plasma Physics and Controlled Fusion*, 63(3):035024, jan 2021.

[22] M. Hoppe, O. Embréus, R.A. Tinguely, R.S. Granetz, A. Stahl, and T. Fülöp. SOFT: a synthetic synchrotron diagnostic for runaway electrons. *Nuclear Fusion*, 58(2):026032, jan 2018.

[23] M. Hoelzl, G.T.A. Huijsmans, S.J.P. Pamela, M. Bécoulet, E. Nardon, F.J. Artola, B. Nkonga, C.V. Atanasiu, V. Bandaru, A. Bhole, D. Bonfiglio, A. Cathey, O. Czarny, A. Dvornova, T. Fehér, A. Fil, E. Franck, S. Futatani, M. Gruca, H. Guillard, J.W. Haverkort, I. Holod, D. Hu, S.K. Kim, S.Q. Korving, L. Kos, I. Krebs, L. Kripner, G. Latu, F. Liu, P. Merkel, D. Meshcheriakov, V. Mitterauer, S. Mochalskyy, J.A. Morales, R. Nies, N. Nikulsin, F. Orain, J. Pratt, R. Ramasamy, P. Ramet, C. Reux, K. Särkimäki, N. Schwarz, P. Singh Verma, S.F. Smith, C. Sommariva, E. Strumberger, D.C. van Vugt, M. Verbeek, E. Westerhof, F. Wieschollek, and J. Zielinski. The JOREK non-linear extended MHD code and applications to large-scale instabilities and their control in magnetically confined fusion plasmas. *Nuclear Fusion*, 61(6):065001, may 2021.

[24] V. Bandaru, M. Hoelzl, F. J. Artola, G. Papp, and G. T. A. Huijsmans. Simulating the nonlinear interaction of relativistic electrons and tokamak plasma instabilities: Implementation and validation of a fluid model. *Phys. Rev. E*, 99:063317, Jun 2019.

[25] Pavel Aleynikov and Boris N. Breizman. Generation of runaway electrons during the thermal quench in tokamaks. *Nuclear Fusion*, 57(4):046009, feb 2017.

[26] Cédric Reux, Carlos Paz-Soldan, Pavel Aleynikov, Vinodh Bandaru, Ondrej Ficker, Scott Silburn, Matthias Hoelzl, Stefan Jachmich, Nicholas Eidietis, Michael Lehnen, Sundaresan Sridhar, and JET contributors. Demonstration of safe termination of megaampere relativistic electron beams in tokamaks. *Phys. Rev. Lett.*, 126:175001, Apr 2021.

[27] A. Loarte, V. Riccardo, J.R. Martin-Solís, J. Paley, A. Huber, and M. Lehnen and. Magnetic energy flows during the current quench and termination of disruptions with runaway current plateau formation in JET and implications for ITER. *Nuclear Fusion*, 51(7):073004, may 2011.

[28] VE Lukash, AA Kavin, Y Gribov, RR Khayrutdinov, and A Loarte. Study of iter plasma position control during disruptions with formation of runaway electrons. In *Proc. 40th EPS Conf. on Plasma Physics (Espoo, Finland, 2013) P5. 167 http://ocs. ciemat. es/EPS2013PAP/pdf.* P5, 2013.

[29] S Konovalov, P Aleynikov, K Aleynikova, Yu Gribov, and R Ismailov. Assessment of the runaway electron energy dissipation in iter. In *26th IAEA Fusion Energy Conference-IAEA CN-234/Programme, TH/7*, 2016.